ACS Macro Letters

Letter

pubs.acs.org/macroletters

Directed Self-Assembly of Lamellar Copolymers: Effects of Interfacial Interactions on Domain Shape

Ginusha M. Perera,[†,‡] Chengqing Wang,[†,§,∥] Manolis Doxastakis,[*,‡] R. Joseph Kline,[*,§] Wen-li Wu,[*,§] August W. Bosse,[*,§] and Gila E. Stein[*,‡]

[‡]Department of Chemical and Biomolecular Engineering, University of Houston, Houston, Texas 77204-4004, United States

[§]Polymers Division, National Institute of Standards and Technology, Gaithersburg, Maryland 20899, United States

Supporting Information

ABSTRACT: The depth-dependent structure of a poly(styrene-*b*-methylmethacrylate) (PS-PMMA) line grating (46 nm pitch) was calculated from quantitative analysis of small-angle X-ray scattering profiles. These data demonstrate that domain shapes are significantly deformed near the substrate interface, where the local PS domain shape resembles an hourglass. The bulk equilibrium dimension is recovered near the center of a 64 nm thick film. Simulations based on self-consistent field theory suggest that deformations near the substrate are caused by extensive penetration of the copolymer domains into the underlying substrate coating (a PS-brush). These findings suggest that new coatings for block copolymer directed self-assembly should consider copolymer penetration lengths in addition to tailoring surface energetics. Furthermore, given the resolution and ensemble-averaging features of synchrotron X-ray scattering, we argue that it has the potential to emerge as a "gold-standard" or "benchmark" dimensional metrology and library validation tool for high density, sub-10 nm features.

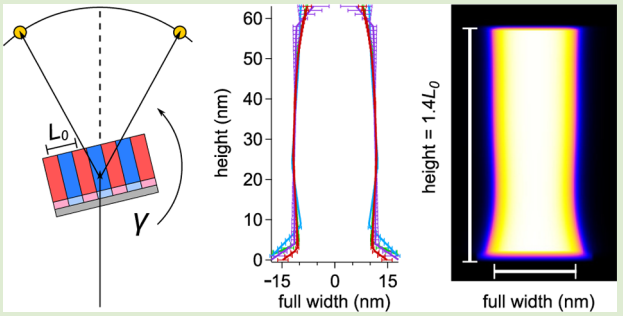

The performance of semiconductor devices is determined by the density of patterned features, whether it be individual transistors in a microprocessor or discrete bits in a high-capacity hard disk drive. As the sizes of patterned features approach 10 nm, the nanopatterning industry is looking to augment traditional optical lithography with new materials and processes. There are a handful of candidate "alternative" technologies competing at the 10 nm node, including direct-write electron beam lithography, extreme ultraviolet lithography, nanoimprint lithography, and directed self-assembly (DSA) of block copolymers. Each of these alternative lithographic techniques will likely enter the manufacturing process as a complement to established lithographic tools.[1,2] For example, DSA can improve the quality of optically patterned resists by shrinking pattern dimensions, increasing pattern density and potentially "healing" defects.[3−7] However, there is evidence from simulations[8] and experiments[9,10] that polymer−substrate interactions can deform the domain shapes. This behavior can be challenging for manufacturing because domain widths must be uniform throughout the film thickness for reliable pattern transfer by plasma etching. In this letter, we use transmission small-angle X-ray scattering (SAXS) to measure the cross sections of poly(styrene-*b*-methyl methacrylate) (PS-PMMA) line gratings. Experimental data are interpreted with the aid of numerical simulations based on self-consistent field theory (SCFT). The concerted experimental and modeling effort demonstrates that DSA pattern quality is strongly affected by the types of interactions at each interface.

In general, the measurement, characterization, and inspection of 10 nm features poses a significant challenge. Traditional microscopy techniques are unreliable because they examine a small subset of the entire sample, are most sensitive to the sample surface, and have established resolution problems at the 10 nm scale. Optical methods such as scatterometry need *validated* measurement libraries for data analysis, so it is difficult to extend these metrologies to new materials and processes. On the other hand, transmission SAXS can resolve the full three-dimensional shape of periodic nanopatterns with high spatial resolution (e.g., <1 nm). Furthermore, SAXS is an *ensemble-averaged* measurement, so meaningful statistical information can be extracted from these data without the need for numerous repeat experiments. Synchrotron X-ray scattering has the potential to emerge as a "gold-standard" or "benchmark" dimensional metrology and library validation tool for high density, sub-10 nm features.

The samples considered in this report are thin films of lamellar PS-PMMA copolymers cast on chemo-epitaxial templates. The PS-PMMA copolymer was purchased from Polymer Source with a number average relative molecular mass of $M_n \simeq 100$ kg/mol, polydispersity index of 1.19, and composition of 52% PS by volume (see Supporting Information). The equilibrium lamellar periodicity is L_0 = (46

Received: June 29, 2012
Accepted: October 5, 2012
Published: October 10, 2012

± 1) nm at 240 °C.[9,11] All copolymer films were (64 ± 1) nm thick and annealed at 240 °C for 6.5 min. The epitaxial templates were fabricated with electron-beam lithography and consist of alternating hydrophobic and hydrophilic lines with a 46 nm pitch, where hydrophobic patterns are PS brush (PS-attractive) and hydrophilic stripes are oxidized PS brush (PMMA-attractive). Atomic force microscopy measurements of patterned brushes are included in the Supporting Information, and these data demonstrate that oxidation induces a subtle change in topography (less than 1 nm height variation). Based on measurements of the electron beam resist profiles, the width of the PS-selective stripe is estimated to range from $w_{PS} \approx 0.55L_0 - 0.63L_0$.[9] Figure 1a includes a schematic of the PS-PMMA line grating and a representative micrograph of the film surface.

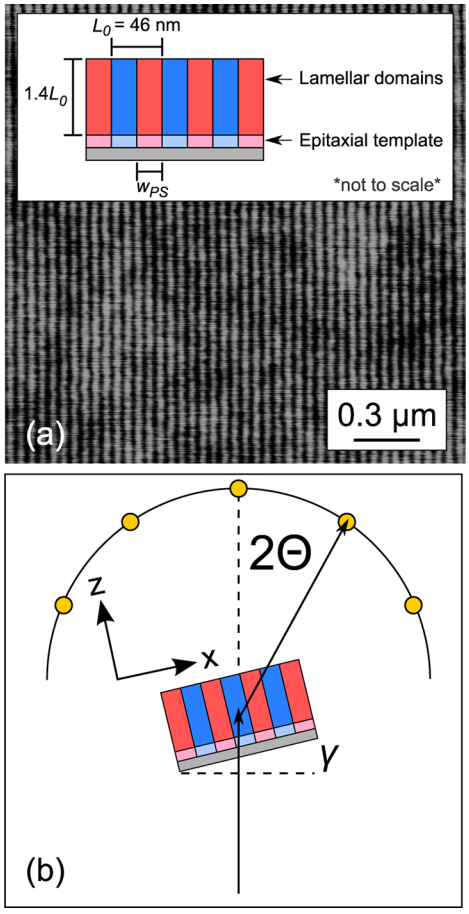

Figure 1. (a) Tapping-mode atomic force microscopy measurement of the block copolymer grating (height image). Dark and bright domains are PS and PMMA, respectively,[11] where PMMA domains are up to 2 nm taller than PS in some regions. This attribute has been observed in other studies of PS-PMMA block copolymers on *homogeneous* surfaces.[11,12] Inset: Schematic of the sample cross-section. (b) Illustration of SAXS geometry.

The structure of PS-PMMA line gratings was characterized with variable-incident-angle SAXS, also known as "critical-dimension" SAXS.[13,14] The measurement geometry is illustrated in Figure 1b. The sample is illuminated at an angle of incidence γ, which is varied through a range of ±45° for depth sensitivity,[14] and the scattered intensity is recorded as a function of diffraction angle 2Θ. All data are mapped from $I(2\Theta, \gamma)$ to $I(q_x,q_z)$ coordinates for comparison with scattering models. Figure 2a includes an example of the data extracted from a single SAXS measurement, and Figure 2b–f reports the scattering profiles $I(q_z)$ for five orders of diffraction peaks $q_x = 2\pi n/L_0$. The three-dimensional shape of the PS-PMMA lamellae was calculated from SAXS data through an inverse solution method. First, the lamellar structure was described by a model that includes the size, shape, and periodicity of the domains, as well as the apparent width of the copolymer interface.[9] The line shape $s(x, z)$ is approximated by a stack of four trapezoids, as illustrated in Figure 3a. The surface topography has little impact on the predicted SAXS intensity, so this structure is not included in the line shape model. This point is further discussed in the Supporting Information. Second, model parameters were refined to obtain agreement between predicted and measured SAXS profiles. This refinement was implemented with a simulated annealing (Monte Carlo) algorithm[15] as gradient search methods were often trapped in local minima, yielding unreliable results that largely depended on the initial values. We performed 150 simulations to collect a family of profiles that were compared with the measured scattering spectra, where a heating/cooling cycle ensured that outcomes from different runs were not correlated. The solid line in Figure 2b–f is the average predicted scattering profile with error bars encompassing ±1 standard deviation.

Figure 3b reports the block copolymer domain shapes that were extracted through analysis of SAXS data. Each curve represents the average line shape with error bars that encompass ±1 standard deviation. When calculating the shape function from SAXS data, there are two planes of symmetry that lead to degenerate solutions, so one cannot distinguish between up/down (180° rotation about the x-plane) or left/right (180° rotation about the z-plane). Therefore, all $s(x, z)$ profiles in Figure 3b were geometrically transposed to overlap. The dimensions of the epitaxial template are different for each sample, but the resulting domain shapes are strikingly similar. All samples exhibit a large "foot" near one interface and a more subtle "rounding" near the other. One could infer that the large "foot" is associated with PS domains wetting the wide PS-attractive stripe. In the center of the film, the domain half-width of all samples is (11.6 ± 0.1) nm, which is the bulk equilibrium dimension. We conclude that interactions at each interface are deforming the domain shapes, and these effects decay with depth into the film interior.

To assist in interpretation of SAXS data, we performed two-dimensional SCFT simulations of symmetric *AB* diblock copolymers confined between a hard substrate and a stationary copolymer–air interface, where both the substrate and the air were modeled using fixed "particles" and implemented in the SCFT simulations as a fixed particle field or masking field.[17] Details of the SCFT framework used here can be found in numerous recent publications;[17–19] here we provide a brief summary of the most salient features. The substrate–copolymer interface was modeled as a relatively diffuse gradient between the pure particle/substrate phase and the pure copolymer melt phase. The substrate interfacial region was approximately 1.4–3 nm wide, depending on the simulation, corresponding to a brush layer that allows for very little to significant copolymer penetration, respectively. The substrate was defined to have two different chemical selectivities, consistent with the chemically patterned substrate in the real PS-PMMA films. The air–polymer interface was modeled using a fixed copolymer gradient with a width of approximately 1.4 nm.

dx.doi.org/10.1021/mz300331k | *ACS Macro Lett.* 2012, 1, 1244–1248

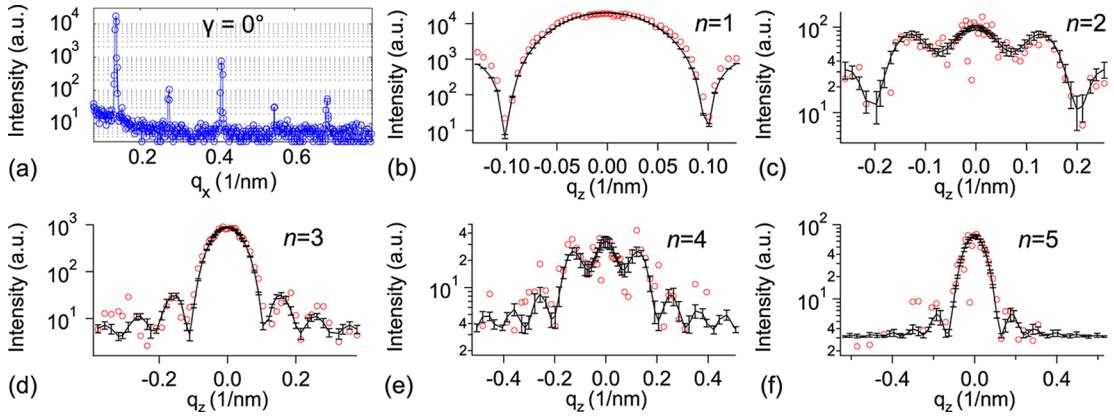

Figure 2. (a) Line profile $I(q_x)$ from data acquired at $\gamma = 0$ ($q_z \approx 0$). Five orders of diffraction peaks are observed, along with weak satellites that are associated with noise in the epitaxial template.[16] (b–f) $I(q_z)$ for five diffraction orders, that is, $q_x = 2\pi n/L_0$. Open symbols are experimental data, and solid line is the best-fit line shape model.

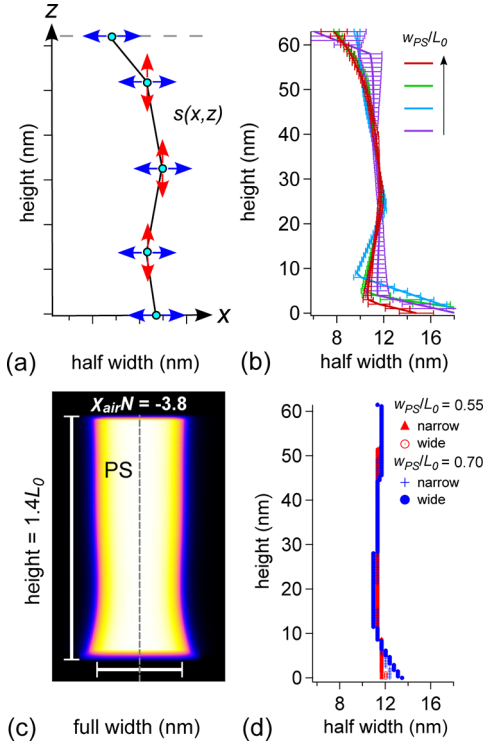

Figure 3. (a) Line shape model $s(x, z)$ for analysis of SAXS data. The total height is constrained, but the height, width, and slope for each trapezoid can vary as illustrated by the arrows. (b) Block copolymer domain shape calculated from SAXS analysis. (c) Simulated domain shape for $w_{PS}/L_0 = 0.7$ with a diffuse copolymer–brush interface. (d) Simulated domain shape for pattern duty cycles of $w_{PS}/L_0 = 0.55$ and $w_{PS}/L_0 = 0.7$, where "narrow" and "wide" denote sharp and diffuse copolymer–brush interfaces, respectively.

With these definitions, there were four independent model parameters, χN, $\chi_{PS}N$, $\chi_{OPS}N$, and $\chi_{air}N$. Here N is the index of polymerization; χ is the A–B Flory parameter; and χ_{PS}, χ_{OPS}, and χ_{air} are composite Flory parameters for the AB copolymer and the PS brush, the partially oxidized PS brush, and the air interface, respectively. The composite Flory parameter for the PS brush is defined such that $\chi_{PS} = (\chi_{PS,A} - \chi_{PS,B})/2$, where $\chi_{PS,A}$ is the Flory parameter for the PS brush and the A segments, and $\chi_{PS,B}$ is the Flory parameter for the PS brush and the B segments. There are similar definitions for χ_{OPS} and χ_{air}. Positive values of the composite Flory parameters indicate an energetic propensity to prefer B segments, while negative values indicate an energetic propensity to prefer A segments.

For all simulations, $\chi N = 38$. This value of χN is consistent with our previous work.[9] The value of $\chi_{air}N$ was selected to be $\chi_{air}N = -3.8$, consistent with an air interface that is slightly preferential toward A segments. Therefore, we identify the A segments in the simulations with the PS segments in the real BCP film. The values of $\chi_{PS}N$ and $\chi_{OPS}N$ were selected to capture the effects of the substrate–BCP interactions. Accordingly, $\chi_{PS,A}N = 0$ and $\chi_{PS,B}N = 38$, while we set $\chi_{OPS,A}N = 38$ and $\chi_{OPS,B}N = -38$; thus, we have $\chi_{PS}N = -19$ and $\chi_{OPS}N = 38$.

The equilibrium pitch of the AB BCP was determined to be $L_0 = 2\pi/k_0 \approx 4.7R_g$, where R_g is the BCP radius of gyration, and k_0 is the location of the primary peak in the simulated structure factor $S(k) \propto |\phi_k|^2$, where ϕ is the simulated local A segment fraction.[20] The simulation space was defined to be approximately one unit cell wide, so that $L_x = 4.7R_g \approx L_0$. The film thickness was selected to be $L_y \approx 1.4L_0 = 6.58R_g$, consistent with the real BCP film. Finally, the spatial resolution for the SCFT simulations was $\Delta x = \Delta y \approx 0.04R_g$ with $2^5 = 32$ points along the copolymer backbone. The SCFT relaxation process also requires defining an effective "time step" for both the pressure and exchange field relaxations.[18] In all SCFT simulations, we used $\Delta t = 4$.[21]

Figure 3c,d reports the simulations for PS domains assembled on a PS-attractive stripe with dimensions of $w_{PS} = 0.55L_0$ and $w_{PS} = 0.7L_0$. It is important to note that domain widths at the substrate interface do not match the template width w_{PS}, but are closer to the equilibrium dimension (ca. $L_0/2$). To induce a local domain deformation that matches w_{PS}, an unreasonably high value of χ_{OPS} must be specified in the simulations. With this in mind, the simulated domain shapes agree qualitatively with experimental data and capture the large "foot." This feature is *potentially* explained by the diffuse brush–copolymer interface, suggesting the copolymer penetrates the brush layer to produce an A–B interface with a pronounced splay at the substrate. We note that several experimental works have demonstrated that copolymer domains can penetrate an underlying brush and interact with the substrate.[11,22,23] We tested this hypothesis by simulating a similar BCP cross section with a much sharper copolymer–substrate interface (Figure 3d). In this scenario, a pronounced

dx.doi.org/10.1021/mz300331k | ACS Macro Lett. 2012, 1, 1244–1248

foot was not observed because significant copolymer penetration into the brush layer was not possible.

The SCFT simulations do not predict significant rounding of the domain shape near the copolymer−air interface, yet this feature is needed to fit experimental spectra. We speculate that the top-rounding is due to swelling of the PMMA domain by ambient humidity,[11] which is consistent with the atomic force microscopy height measurement in Figure 1 (where PMMA domains are slightly "taller" than PS). If moisture is responsible for the surface deformations, then one could potentially reverse this effect by heating the films near the glass transition temperature (ca. 100 °C).[11]

While not the principal focus of this letter, we note that the apparent width of the copolymer interface was calculated as part of SAXS data analysis. The apparent interfacial width is a convolution of the mean-field composition profile and thermal fluctuations, which is discussed extensively elsewhere.[24−26] The values extracted for each sample were 4.90 ± 0.02, 4.95 ± 0.02, 4.80 ± 0.02, and 4.90 ± 0.02 nm, in close agreement with prior predictions and measurements for the same PS-PMMA lamellar copolymer.[9] The apparent interfacial width contains information about line-edge roughness, an important metric for semiconductor manufacturing that refers to low-frequency variations in the line-edge position. Ultimately, we intend to extract the line-edge roughness spectrum from the scattering data, as specific frequency ranges have markedly different effects on final device function.[27] Armed with a physically reasonable model for fluctuations and line-edge roughness,[24,26,28,29] one can hope to extract the spectral information from the diffuse scattering around the diffraction peaks in the q_y direction. This is currently a research focus of our groups.

In conclusion, we used transmission SAXS to measure the cross-sectional shape of PS-PMMA line gratings. The experimental data were interpreted with the aid of numerical simulations based on SCFT. The concerted experimental and modeling effort demonstrates that DSA pattern quality is strongly affected by the types of interactions at each interfaces. Specifically, we measured a relatively large "foot" at the copolymer−substrate interface that results in a subtle "neck" and "shoulder" in the grating cross section. SCFT simulations corroborate this observation and suggest that the foot is a result of significant copolymer penetration into the underlying brush layer. These observations are important for lithography scientists because vertical domain sidewalls are needed for optimal pattern transfer. Significantly, these findings suggest that new coatings for DSA should consider copolymer penetration lengths in addition to tailoring surface energetics.

EXPERIMENTAL SECTION

Fabrication of epitaxial templates, characterization of epitaxial templates, and DSA of the PS-PMMA lamellae are discussed elsewhere.[9] These procedures are very similar to work described by Nealey et al.[8] Variable-incident-angle SAXS measurements were implemented at the Advanced Photon Source of Argonne National Laboratory (beamline 8-ID-E). Samples were placed in a vacuum chamber and illuminated with 7.35 keV radiation at incident angles (γ) in the range of −45° to 45° with increments of 1.3°. The beam spot size was 150 μm wide by 50 μm tall. The scattering was recorded with a Pilatus 1MF pixel array detector (pixel size = 172 μm) positioned 2175 mm from the sample. Acquisition times were 10 s per angle. All intensities were corrected to account for changes in illuminated volume as a function of γ. For SAXS data analysis, we calculated the area under each primary peak as function of incident angle γ and scattering angle 2Θ. These data are then mapped to (q_x, q_z) coordinates following the definitions in Figure 1b. All data are background corrected to remove the parasitic scattering at low q_x values. (Certain commercial equipment, instruments, or materials are identified in this paper in order to specify the experimental procedure adequately. Such identification is not intended to imply recommendation or endorsement by the National Institute of Standards and Technology, nor is it intended to imply that the materials or equipment identified are necessarily the best available for the purpose.)

ASSOCIATED CONTENT

Supporting Information

(i) Atomic force microscopy measurements of nanopatterned PS brushes; (ii) Characterization of the PS-PMMA copolymer; (iii) SAXS data modeled with a form factor that includes surface topography. This material is available free of charge via the Internet at http://pubs.acs.org.

AUTHOR INFORMATION

Corresponding Author

*E-mail: edoxastakis@uh.edu; joe.kline@nist.gov; wen-li.wu@nist.gov; august.bosse@nist.gov; gestein@uh.edu.

Present Address

[‖]KLA-Tencor, One Technology Drive, Milpitas, California 95035, United States.

Author Contributions

[†]Equal contribution.

Notes

The authors declare no competing financial interest.

ACKNOWLEDGMENTS

G.E.S. and G.M.P. acknowledge financial support by the National Science Foundation under Grant No. EEC/ECCS-0927147 and the UH GEAR Award No. 98520. M.D. acknowledges financial support by the National Science Foundation under Grant No. CBET 1067356. C.W., A.W.B., R.J.K., and W.W. acknowledge the support of the members of the Energy and Electronics Materials Group and the Theory, Modeling, and Simulation Working Group, both in the Polymers Division at the National Institute of Standards and Technology (NIST). This work made use of the NIST Material Measurement Laboratory central computing facilities in the Center for Theoretical and Computational Materials Science. Electron-beam patterning was performed at the NIST Center for Nanoscale Science and Technology. Use of the Advanced Photon Source was supported by the U.S. Department of Energy, Office of Science, Office of Basic Energy Sciences, under Contract No. DE-AC02-06CH11357. We thank Joseph Strzalka for assistance with SAXS measurements and Mike Nikolaou for helpful discussions regarding numerical methods.

REFERENCES

(1) Cheng, J. Y.; Sanders, D. P.; Truong, H. D.; Harrer, S.; Friz, A.; Holmes, S.; Colburn, M.; Hinsberg, W. D. *ACS Nano* **2010**, *4*, 4815−4823.

(2) International technology roadmap for semiconductors; 2011, http://www.itrs.net/.

(3) Kim, S.; Solak, H.; Stoykovich, M.; Ferrier, N.; de Pablo, J.; Nealey, P. *Nature* **2003**, *424*, 411−414.

(4) Stoykovich, M.; Muller, M.; Kim, S.; Solak, H.; Edwards, E.; de Pablo, J.; Nealey, P. *Science* **2005**, *308*, 1442−1446.

(5) Stoykovich, M. P.; Kang, H.; Daoulas, K. C.; Liu, G.; Liu, C.-C.; de Pablo, J. J.; Mueller, M.; Nealey, P. F. *ACS Nano* **2007**, *1*, 168−175.

(6) Cheng, J. Y.; Rettner, C. T.; Sanders, D. P.; Kim, H.-C.; Hinsberg, W. D. *Adv. Mater.* **2008**, *20*, 3155−3158.
(7) Stoykovich, M. P.; Daoulas, K. C.; Mueller, M.; Kang, H.; de Pablo, J. J.; Nealey, P. F. *Macromolecules* **2010**, *43*, 2334−2342.
(8) Edwards, E. W.; Mueller, M.; Stoykovich, M. P.; Solak, H. H.; de Pablo, J. J.; Nealey, P. F. *Macromolecules* **2007**, *40*, 90−96.
(9) Stein, G. E.; Liddle, J. A.; Aquila, A. L.; Gullikson, E. M. *Macromolecules* **2010**, *43*, 433−441.
(10) Liu, G.; Kang, H.; Craig, G. S. W.; Detcheverry, F.; de Pablo, J. J.; Nealey, P. F.; Tada, Y.; Yoshida, H. *J. Photopolym. Sci. Technol.* **2010**, *23*, 149−154.
(11) Vu, T.; Mahadevapuram, N.; Perera, G. M.; Stein, G. E. *Macromolecules* **2011**, *44*, 6121−6127.
(12) Thurn-Albrecht, T.; Steiner, R.; DeRouchey, J.; Stafford, C.; Huang, E.; Bal, M.; Tuominen, M.; Hawker, C.; Russell, T. *Adv. Mater.* **2000**, *12*, 787−791.
(13) Jones, R.; Hu, T.; Lin, E.; Wu, W.; Kolb, R.; Casa, D.; Bolton, P.; Barclay, G. *Appl. Phys. Lett.* **2003**, *83*, 4059−4061.
(14) Hu, T.; Jones, R.; Wu, W.; Lin, E.; Lin, Q.; Keane, D.; Weigand, S.; Quintana, J. *J. Appl. Phys.* **2004**, *96*, 1983−1987.
(15) Kirkpatrick, S.; Gelatt, C.; Vecchi, M. *Science* **1983**, *220*, 671−680.
(16) Perera, G. M.; Stein, G. E.; Liddle, J. A. *J. Vac. Sci. Technol., B* **2010**, *28*, 1048−1055.
(17) Matsen, M. *J. Chem. Phys.* **1997**, *106*, 7781−7791.
(18) Fredrickson, G.; Ganesan, V.; Drolet, F. *Macromolecules* **2002**, *35*, 16−39.
(19) Bosse, A. W.; Garcia-Cervera, C. J.; Fredrickson, G. H. *Macromolecules* **2007**, *40*, 9570−9581.
(20) The equilibrium pitch of the BCP was calculated using a bulk SCFT simulation with χN = 38.
(21) The pressure field was updated using a first-order accurate, explicit Euler method, and the exchange field was updated using a first-order accurate, semi-implicit Euler method.
(22) Mansky, P.; Russell, T.; Hawker, C.; Mays, J.; Cook, D.; Satija, S. *Phys. Rev. Lett.* **1997**, *79*, 237−240.
(23) Guo, R.; Kim, E.; Gong, J.; Choi, S.; Ham, S.; Ryu, D. Y. *Soft Matter* **2011**, *7*, 6920−6925.
(24) Semenov, A. N. *Macromolecules* **1993**, *26*, 6617−6621.
(25) Shull, K. R.; Mayes, A. M.; Russell, T. P. *Macromolecules* **1993**, *26*, 3929−3936.
(26) Semenov, A. N. *Macromolecules* **1994**, *27*, 2732−2735.
(27) Yamaguchi, A.; Fukuda, H.; Arai, T.; Yamamoto, J.; Hirayama, T.; Shiono, D.; Hada, H.; Onodera, J. *J. Vac. Sci. Technol., B* **2005**, *23*, 2711−2715.
(28) Bosse, A. W. *J. Vac. Sci. Technol., B* **2011**, *29*, 06F202.
(29) Bosse, A. W. *Phys. Rev. E* **2012**, *85*, 042801.